This is a repository copy of *Control of the porous structure of polystyrene particles obtained by nonsolvent induced phase separation*.

White Rose Research Online URL for this paper:
https://eprints.whiterose.ac.uk/123865/

Version: Accepted Version

CONTROL OF THE POROUS STRUCTURE OF POLYSTYRENE PARTICLES OBTAINED BY NON-SOLVENT INDUCED PHASE SEPARATION

Antonino Bianco[1,2], Stephanie L. Burg[3], Andrew J. Parnell[3], Christine M. Fernyhough[2], Adam L. Washington[3], Christopher J. Hill[4], Patrick J. Smith[2], David M. Whittaker[3], Oleksandr O. Mykhaylyk[1], J. Patrick. A. Fairclough[2].

[1] Department of Chemistry, The University of Sheffield, S3 7HF, UK.

[2] Department of Mechanical Engineering, The University of Sheffield, S3 7HQ, UK.

[3] Department of Physics and Astronomy, The University of Sheffield, S3 7RH, UK.

[4] Department of Biomedical Science, The University of Sheffield, S10 2TN, UK.

ABSTRACT. Porous polystyrene micro-spheres were produced by a process of non-solvent induced phase separation (NIPS) from ternary polymer-solvent-non solvent (polystyrene-toluene-ethanol) systems and characterised by scanning electron microscopy (SEM) and small angle X-ray scattering (SAXS) techniques. This study provides evidence for a link between the structural morphology of the porous polystyrene particles and the polystyrene concentration in the initial solutions. A reciprocal relationship between pore diameter and polymer concentration was observed for the systems with the polymer amount below the critical chain overlap concentration, C^*. Above C^* this relationship breaks down. The reciprocal relationship between porosity and polymer concentration can be used to facilitate the fine control of the voids size. We demonstrate that the observed reciprocal relationship between pore diameter and polymer concentration correlates well with the relative amount of non-solvent present in the system at the onset of the phase separation process. The pore size can be reduced and, consequently, the pore surface area can be increased either by reducing the polymer concentration in the initial solution or by decreasing the polymer molecular weight in the sample composition.

INTRODUCTION.

Porous polymer structures are of great interest due to their application in many industrial areas, from the preparation of filtration systems,[1,2] to their use as tissue scaffolds,[3,4,5] carriers for catalysts,[6] adsorbents for heavy metal removal from aqueous solutions[7] and for controlled drug release,[8] to cite a few.

Porosity may be achieved in different classes of structures, such as large monoliths,[1] thin membranes[9] or micro-spheres.[10] There are a number of synthetic methods for producing organic porous materials.[11,2] In particular, porous polymers can be obtained by exploiting the process of phase separation of an initially homogeneous polymer solution.[12] Phase separation takes place when there is an increase in the Gibbs free energy of the system. This favours the de-mixing of the polymer solution, which can be induced by a change in temperature (thermally induced phase separation, TIPS) or by the introduction of a non-solvent (non-solvent induced phase separation, NIPS).[13,14] The latter is the focus of this study.

Research on polycarbonate NIPS to manufacture porous monoliths, highlighted the impact of different molecular weights and polymer concentrations on the final morphology achieved.[1] Polycarbonate polymers of different molecular weights were dissolved in chloroform, with cyclohexane acting as the non-solvent to induce phase separation.[1]

This study showed empirical correlations in the pore size from increasing polymer molecular weight, the non-solvent ratio, reduction in temperature, all causing a decrease in the pore size. The authors explained this dependence with the viscosity of the systems, as they suggested that the viscosity would strongly affect the phase separation process and the resulting void size.[1]

The importance of the specific solvent for achieving a set pore morphology has also been examined.[15] Two NIPS systems based on poly-(methyl methacrylate), with either N,N-dimethylformamide (DMF) or acetone as the solvent, and water as the non-solvent, were studied.[15]

The DMF system corresponded to a rapid de-mixing of the polymer solution, due to the water having high affinity for DMF. In the acetone system a delayed de-mixing occurred, due to water having a lower affinity for acetone compared to DMF.

As a result of the different affinities between solvent and non-solvent, and therefore different exchange rates between them, different pore morphologies were observed: elongated pores were achieved for membranes produced with DMF, while spherical pores were observed in membranes with acetone.[15]

A combination of both TIPS and NIPS has been used to produce porous micro-granules of polystyrene.[7] In this instance the polymer was dissolved in cyclohexane and heated to a temperature in the range of 50-60 °C. An emulsion of this solution was formed by dispersing the solution in water, and stabilised by a surfactant. This emulsion was then mixed with the non-solvent ethanol at 0 °C. The concentration of polystyrene in solution, affecting the viscosity of the system and the solvent-non solvent exchange rate, was found to have a major impact on the morphology of the polystyrene structures.[7]

Low concentration solutions of polystyrene favoured the formation of polymer nuclei with low porosity. An intermediate polystyrene concentration favoured a continuous network morphology within the particles, whilst high polystyrene concentrations produced spherical micro-granules with large internal cavities.[7]

Due to the broad range of porous structures that can be achieved, phase separation of a homogeneous polymer solutions is a widely studied process which can be understood thermodynamically.[13] However, the kinetics of the process also plays an important role.

The Gibbs energy of mixing in a polymer-solvent system is described by the Flory-Huggins equation:[13]

$$\Delta G = RT \left(n_1 \ln \phi_1 + n_2 \ln \phi_2 + n_1 \, \phi_2 \, \chi_{12} \right) \tag{1}$$

where R is the gas constant, T is the temperature, n_2 is the number of moles of polymer, n_1 is the number of moles of the solvent, ϕ_2 is the volume fraction of the polymer, ϕ_1 is the volume fraction of the solvent, χ_{12} is the Flory-Huggins interaction parameter between the polymer and the solvent which can be approximated as:[13]

$$\chi_{12} = \frac{V_r}{RT} \left(\delta_1 - \delta_2 \right)^2 \tag{2}$$

where V_r is the reference molar volume, usually of the solvent, δ_1 and δ_2 are the solubility parameters for solvent and polymer respectively.

Upon the introduction of a third component, the non-solvent, the equation (1), corresponding to a binary system, is modified with extra terms describing the effect of the non-solvent in order to express the Gibbs energy of mixing of the ternary system comprising polymer, solvent and non-solvent:[13]

$$\Delta G = RT \left(n_1 \ln \phi_1 + n_2 \ln \phi_2 + n_1 \phi_2 \chi_{12} + n_3 \ln \phi_3 + n_3 \phi_2 \chi_{23} + n_3 \frac{\phi_1}{\phi_1 + \phi_3} \phi_1 \chi_{13} \right) \qquad (3)$$

where n_3 refers to the number of moles of the non-solvent, ϕ_3 to the volume fraction of the non-solvent, χ_{13} is the interaction parameter for the solvent-non solvent and χ_{23} is the interaction parameter for the polymer-non solvent.[13] Thus the thermodynamic driving force during NIPS is related to the interaction parameters and the component concentrations.

The phase separation of the homogeneous polymer solution takes place when the free energy of a two-phase system is lower than the free energy of the corresponding single-phase system. The de-mixing produces polymer-rich and polymer-poor phases that result in a polymer matrix with internal porosity.[12] [13] In practice the thermodynamics of phase separation is intrinsically linked with the kinetics of solvent exchange. As the solvent is replaced by the non-solvent, a concentration wave sweeps through the system. At one side the system is thermodynamically stable, at the other the system undergoes phase separation.[16] At some point in the phase separation the structure within the system is pinned and motion is arrested. This arrest of motion can be due to a glass transition temperature, crystallisation or hydrogen bonding. This arrest ultimately controls the final structure observed experimentally. The rate of solvent mixing is high because of the high mobility of the solvent molecules in the polymer matrix (analogous to cyclist in traffic): the majority of the small solvent molecules are not constrained and can move freely in the swollen polymer. However, the polymer is restricted by interactions with itself or other polymer molecules.

Thus, every ternary system has a characteristic phase separation behaviour that is related to factors such as the Flory-Huggins interaction parameter, the polymer molecular weight and polymer concentration, solvent to non-solvent ratio and their relative miscibility.

A numerical method was developed for the construction of ternary phase diagrams based on the Flory-Huggins theory.[17,18] By taking into consideration binary interaction parameters, ternary phase diagrams describing the behaviour of polymer-solvent-non solvent systems at a given temperature were constructed.[17]

One of the ternary systems investigated was a cellulose acetate, dioxane, water system. The theoretical position for the binodal line was compared to the experimentally determined binodal, obtained by cloud point measurements of the system at different polymer concentrations and temperatures.

It was found that the experimentally determined binodals for cellulose acetate with M_w between 9 and 30 kg mol^{-1} obtained by cloud point measurements at 20 °C and at 60 °C were in reasonably good agreement with the theoretical binodal predicted by the numerical model.[17]

The behaviour of a ternary system can be generalised by a comprehensive phase diagram (Figure 1).[19]

Figure 1. A generic ternary phase diagram describing the behaviour of a polymer-solvent-non solvent system at a given temperature. The binodal line marks the boundary between the one-phase region, where the system is a homogenous solution, and the two-phase region, where the system transforms into a liquid-liquid mixture and further into a solid-liquid mixture as progressively more non-solvent is added. The upper limit of the binodal is referred to as the critical point C. The spinodal line, which is the boundary between metastable and unstable zones in the two-phase region, is also shown. The Berghman's Point B marks the limit where the glass transition

temperature of the polymer is lower than the temperature of the system. Beyond the B-point phase separation stops and particles morphology is retained. (Re-drawn from Wang et al. [19]).

At a given temperature, when non-solvent is added to the polymer solution, the system transitions from the one-phase region across the binodal line to the two-phase region. This results in the formation of polymer-poor and polymer-rich regions within the polymer mixture.[12] With continuing progress into the non-solvent quenching regime, either spinodal decomposition or nucleation and growth processes take place and they arrest at the Berghman's Point B, where the glass transition temperature of the polymer intersects the temperature of the system.[19] The morphology achieved at this stage is thus fixed and observed experimentally.

In polymer solutions with concentrations above the critical chain overlap concentration C^*,[20] the mobility within the system is drastically reduced due to polymer chain entanglement, resulting into a significant increase in viscosity which may have a pronounced effect on the phase separation of the system prior to reaching the Berghman's Point.[20]

The main goal of the current study was to investigate the relationship between the initial polymer solution concentration and the final morphology of the resultant multi-voided polymer particles. Due to its wide availability, low cost and extensive existing literature, polystyrene was chosen as a model polymer for this study. Different molecular weights were investigated, including uni-modals and a bi-modal molecular weight distribution. Polystyrene multi-voided particles were produced by the NIPS process using toluene as the solvent and ethanol as the non-solvent.

An emulsion process was employed in order to increase the control over particles shape and size, as this affects the rate of solvent ingress by diffusion. Different morphologies were achieved by varying the molecular weight of polystyrene and the concentration of the polymer solutions.
The final porous structures achieved were characterised by a combination of scanning electron microscopy (SEM) and small angle X-ray scattering (SAXS).

MATERIALS AND METHODS.

Polystyrene samples with lower, intermediate and higher molecular weights $M_w \approx 23$, 207 and 317 kg mol^{-1}, were purchased either from Polymer Source (Montreal, Canada) and Sigma Aldrich (Gillingham, England). An additional bi-modal polystyrene blend with $M_w \approx 53$ and 107 kg mol^{-1} was purchased from Sigma Aldrich, where it was incorrectly labelled as a 35 kg mol^{-1} sample. Toluene (Chromasolv HPLC grade 99.9%) and non-ionic surfactant Sorbitane monooleate (Span 80) were also purchased from Sigma Aldrich; Ethanol (Analar Normapur) was purchased from VWR Prolabo Chemicals (Hunter Boulevard, England) and deionised water was obtained from a Milli-Q Millipore water system. All materials were used without further purification.

Multi-voided polystyrene particles were fabricated by an emulsion NIPS process, as illustrated in Figure 2. Polystyrene pellets were dissolved in toluene at room temperature in order to produce polymer solutions of the desired weight/weight percentage concentrations (2, 5, 7, 10 and 15% w/w). An amount (2% w/w) of Span 80 non-ionic surfactant was added to the polymer solution and dispersed by magnetic stirring. Water was added in ratio 2 : 1 w/w to the polymer solution and the mixture was stirred at 1000 rpm for 15 minutes to form a stable oil in water emulsion. The emulsion was then transferred to a 60 ml syringe connected to a syringe pump. The flow rate was set to 100 ml/hr in order to deliver the emulsion to a stirring bath of the non-solvent ethanol. The ratio of emulsion to non-solvent was kept close to 1 : 10 w/w for all the samples (this ratio refers to the final state of the system, when all the emulsion has been transferred to the non-solvent bath). The precipitated polystyrene micro-spheres were isolated from the mixture by vacuum filtration and left to dry in a fume cupboard to remove solvent. The samples prepared are named in terms of the polystyrene molecular weights and polystyrene concentrations in the polymer solutions. For example, the products prepared with polystyrene M_w 23 kg mol^{-1} at 2% w/w concentration and M_w 207 kg mol^{-1} at 5% w/w would be referred to as "23-2" and "207-5", respectively.
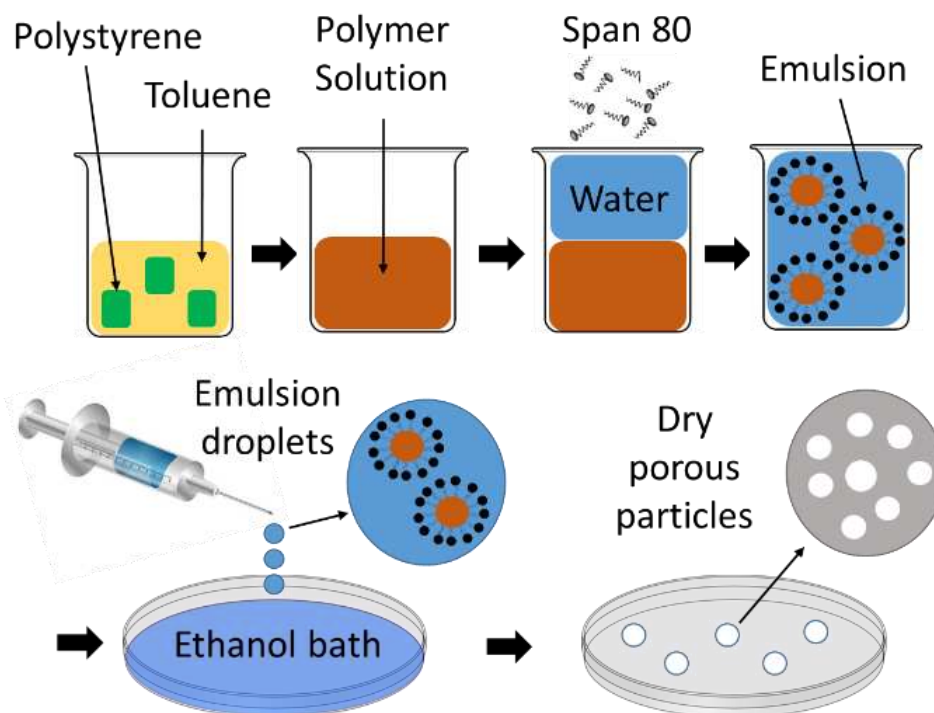
Figure 2. The process of non-solvent induced phase separation (NIPS). Polystyrene in the form of pellets is dissolved in toluene at room temperature in order to produce a polymer solution of desired concentration. Non-ionic surfactant Span 80 and water are added to the polymer solution in order to form an emulsion upon stirring: the polymer solution is dispersed in the form of droplets in a continuous phase of water. The emulsion is delivered dropwise to a bath of ethanol non-solvent. The polystyrene precipitates in the form of porous micro-particles. The particles are isolated by vacuum filtration and left to dry to remove solvent.

The molecular weight of the various polystyrenes studied was measured by Gel Permeation Chromatography (GPC) using triple detection with light scattering. The analysis provided a molecular weight M_w of 207,179 g mol^{-1} with a polydispersity index of 2.095 for the M_w 207 kg mol^{-1} sample (Sigma Aldrich, Lot. number 02726DE) and a M_w of 316,573 g mol^{-1} with a polydispersity index of 2.944 for the M_w 317 kg mol^{-1} sample (Sigma Aldrich, Lot. number MKBP1175V). The bi-modal sample (Sigma Aldrich, Lot. number MKBS6957V) showed two populations of polymer chains with molecular weights M_w of 53,309 and 106,970 g mol^{-1}. The lower M_w sample, 23 kg mol^{-1} (Polymer Source, Lot. Number P9397-S) was analysed with a GPC set-up comprised of two 5 μm "Mixed-C" columns, a WellChrom K-2301 refractive index detector operating at 950 nm, THF eluent containing 2% v/v triethylamine and 0.05% w/v butylhydroxytoluene (BHT) with a flow rate of 1.0 mL min^{-1}, calibrated with standards from Polymer Laboratories (Church Stretton Salop, England). The analysis provided a molecular weight M_w of 23,092 g mol^{-1} with a polydispersity index of 1.244. For more information see the supporting information section.

The droplet size of the emulsions of polystyrene solutions dispersed in water was measured by Dynamic Light Scattering (DLS), using a Malvern Zetasizer Nano-S series instrument with 1 ml cuvettes. The instrument was operated under the following conditions: temperature of 25 °C, detector angle at 90°, incident laser wavelength of 633 nm. DLS has shown that oil-phase droplet size in the emulsions for all the prepared samples was in the size range 20-70 μm.

Cloud points measurements for polystyrene, toluene and ethanol systems were determined by turbidimetric titration method at 25 °C. Ethanol, as non-solvent, was delivered from a burette into continuously stirred solutions of polystyrene in toluene and the turbidity (cloudiness) of the solutions was visually assessed throughout the addition.

The viscoelastic properties of polystyrene, toluene and ethanol systems were measured using a rotational stress-controlled rheometer (Anton Paar, MCR 502) equipped with a cone-and-plate geometry (diameter 50 mm and cone angle 2°) at 25 °C using the continuous shear mode. The dependence of viscosity (η) on shear rate ($\dot{\gamma}$) was measured within $\dot{\gamma}$ intervals from 1 to 100 rad s^{-1}. This range was selected in order to obtain reliable values of zero shear rate viscosity for solutions at low polystyrene concentration. The viscosity η in this range was independent of shear rate. The zero shear viscosity η_o was extrapolated to $\dot{\gamma} = 0$. Time sweeps performed before each run have shown that the effect of solvent evaporation was negligible for the measurements time used.

Structural morphology of polystyrene multi-voided particles was characterised by SEM, using a Philips XL-20 instrument operating at a voltage of 15 kV. Samples were fractured between microscope glass slides in order to image their cross-sections, representing internal structural morphology. The samples were then coated with gold using an Edwards S150B sputter coater. In order to estimate the pore size distribution, the SEM images were analysed using Image J software (version 1.50d).[21,22]

SAXS measurements were either performed at a synchrotron source (ESRF, beamline ID02, Grenoble, France) or using a laboratory SAXS instrument (Xeuss 2.0, Xenocs, France) equipped with liquid gallium MetalJet X-ray source (Excillum, Sweden). A monochromatic X-ray radiation (wavelength $\lambda = 0.0995$ nm or 0.134 nm,

respectively) and 2D detector (Rayonix MX-170HS CCD or Dectris Pilatus 1M pixel detector, respectively) were used for these experiments. The SAXS camera length was set to cover the q range from 0.01 nm^{-1} to 1.0 nm^{-1}, where $q = 4\pi sin\theta/\lambda$ is the modulus of the scattering vector and θ is half of the scattering angle. Glass capillaries (approximate diameter of 2 mm) were used as a sample holder for the dried polystyrene particles. X-ray scattering data were reduced (integration and normalization) using standard routines from the beamline or the software package Foxtrot for the laboratory SAXS instrument. Irena SAS macros[23] for Igor Pro software were utilized for background subtraction and analysed using the Unified fit method.[24]

RESULTS AND DISCUSSION.

Phase diagram of polystyrene-toluene-ethanol ternary systems.

A ternary phase diagram for the polystyrene, toluene and ethanol systems studied was constructed from cloud point measurements (Figure 3). Cloud points were determined by turbidimetric titration at 25 °C.

The volume of ethanol required to achieve cloudiness in solutions of different concentrations of polystyrene were converted into weights. Each point on the ternary diagram (Figure 3) is expressed in weight percentage of polystyrene, toluene and ethanol.

Linking the cloud points provides information on the position of the binodal, the boundary line that separates the one-phase region, where the mixture is homogeneous, from the two-phase region, where the mixture separates into liquid-liquid polymer-rich and polymer-poor regions. With continuing addition of the non-solvent, the polystyrene precipitates.

The initial condition of the systems, for polystyrene toluene solutions at concentrations of 2, 5, 7, 10 and 15% w/w lie on the polystyrene-toluene axis of the diagram (Figure 3, filled triangles). Upon the addition of the non-solvent, the system transfers through the binodal line to the two-phase region, initiating phase separation. The diagram shows the final configuration of the system (Figure 3, filled squares) where ethanol is the dominant component and polystyrene is precipitated in the form of solid porous micro-spheres. The binodal boundary is progressively shifted towards the polystyrene-toluene axis as the polystyrene molecular

weight increases. The obtained phase diagram (Figure 3) is consistent with a generic ternary diagram expected for such a system (Figure 1).
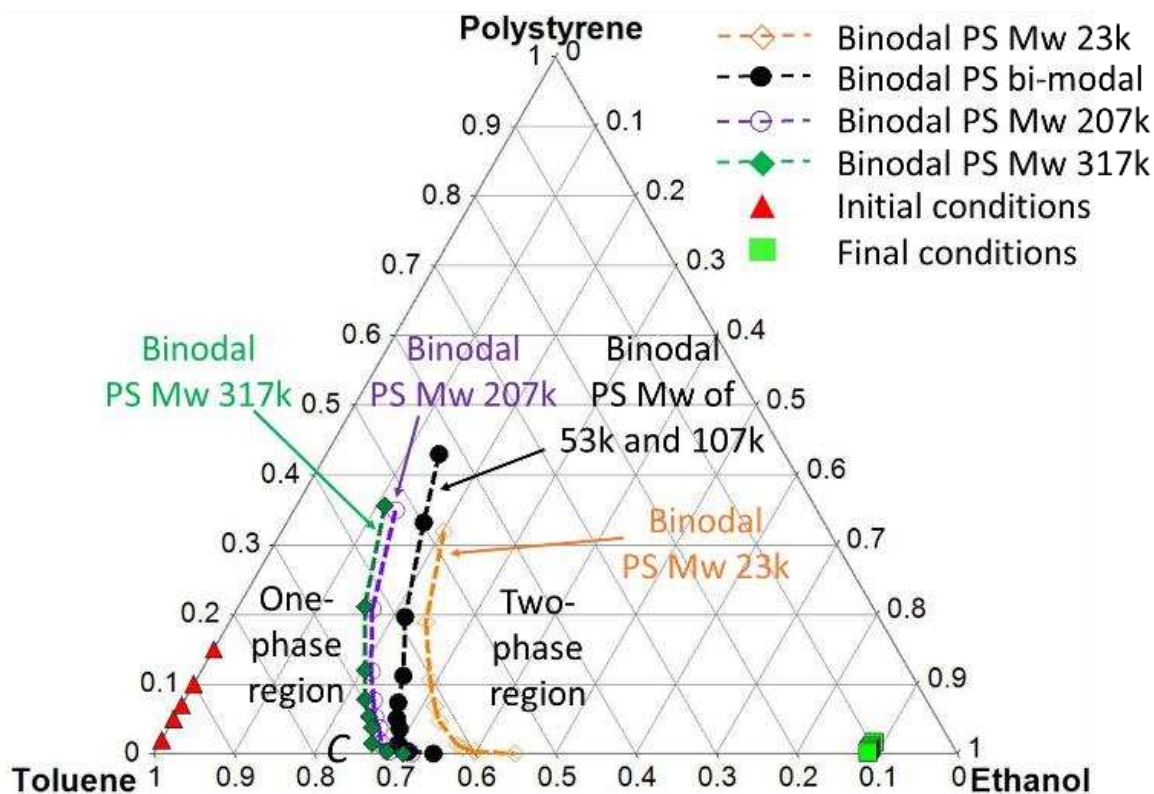

Figure 3. A ternary phase diagram showing the evolution of polystyrene-toluene-ethanol systems at 25 °C. From the initial conditions of polystyrene toluene solutions at PS concentrations of 2, 5, 7, 10 and 15% w/w (triangles) the system transitions to the final state (squares) upon the addition of ethanol non-solvent. Experimentally determined binodal lines, obtained from cloud points, are shown for polystyrene molecular weights of 23 (open diamonds), 207 (open circles), 317 (full diamonds) and bi-modal blend of 53 and 107 (full circles) kg mol^{-1}, marking the boundary between one-phase and two-phase regions. The cloud points were measured up to 40% w/w for PS M_w 23, 207, 317 kg mol^{-1} and 50% w/w for PS bi-modal blend. Beyond these concentrations the solutions were too viscous to perform the analysis. Phase separation occurs when the binodal line is crossed, initially producing a liquid-liquid mixture with polymer-rich and polymer-poor regions and upon further addition of ethanol a solid-liquid mixture occurs where polystyrene precipitates.

Critical chain overlap concentration.

The chain overlap concentration C^* of a homogeneous polymer solution is defined as the critical concentration at which polymer coils begin to overlap.[25]

It is expected that above the critical chain overlap concentration, the mobility of polystyrene systems is drastically reduced due to the increased viscosity.

11

The critical chain overlap concentration can be defined as:[25]

$$C^* = \frac{3M_w}{4\,\pi\,(R_g^2)^{3/2}N_A} \qquad (4)$$

where M_w is the molecular weight of the polymer, R_g^2 is the mean squared radius of gyration of polystyrene in toluene and N_A is the Avogadro's number.

In order to calculate C^* for the polystyrene-toluene systems the values for the radius of gyration R_g of polystyrene in toluene is required.[26] In this respect two approaches have been used (Table 1 and Table 2). The first approach was based on the values reported in the literature[26] (Table 1). The values of R_g chosen for the calculations were those that were the closest to the molecular weights of the studied polystyrene. It was found that for the 23 kg mol⁻¹ series the 15% w/w concentration is the only system above C^*. For the 207 kg mol⁻¹ series the 2% w/w concentration is the only system below C^* and the 317 kg mol⁻¹ series is entirely above C^*. The bi-modal system is below C^* at 2, 5 and 7% and above C^* at 15%, while at 10% the short and long chains are below and above C^* respectively (Table 1).

Table 1. Calculations of C^* using eq. 4 and experimental values of R_g from literature.[26] The systems with the concentrations above C^*, where the phase separation process is kinetically controlled, are highlighted in orange. B = Below C^*, A = Above C^*.

PS Mw	R_g / nm	C^* / g cm³	2%	5%	7%	10%	15%
23k	4.58	0.096	B	B	B	B	A
bi-modal 53k and 107k	5.36 and 8.20	0.136 and 0.077	B	B	B	B/A	A
207k	13.40	0.034	B	A	A	A	A
317k	23.30	0.010	A	A	A	A	A

The second approach used for the C^* calculation is based on the R_g values obtained from the Kuhn length of polystyrene in a theta-solvent.

In this case R_g is calculated from the relation between the contour length and the Kuhn length:[27,28]

$$R_g{}^2 = \frac{1}{6} L \times b \qquad (5)$$

where R_g^2 is the mean squared radius of gyration of polystyrene, b is the Kuhn length of polystyrene (1.67 nm, as reported in literature[28]) and L is the contour length of polystyrene, defined as:

$$L = 2 \times l \times \cos\left(\frac{\theta}{2}\right) \times N \qquad (6)$$
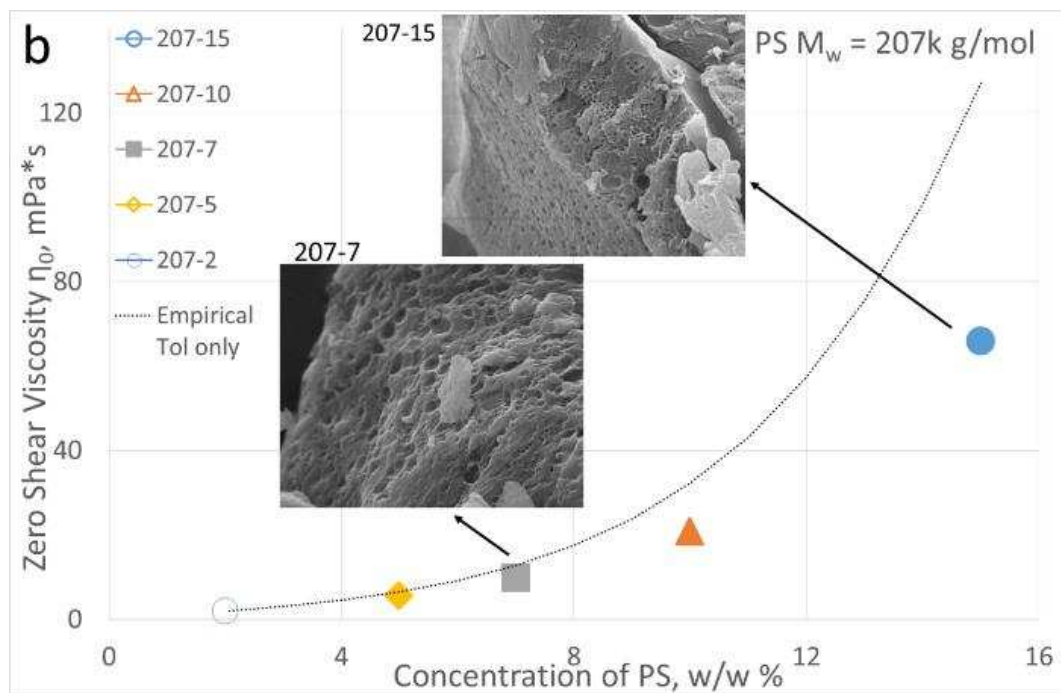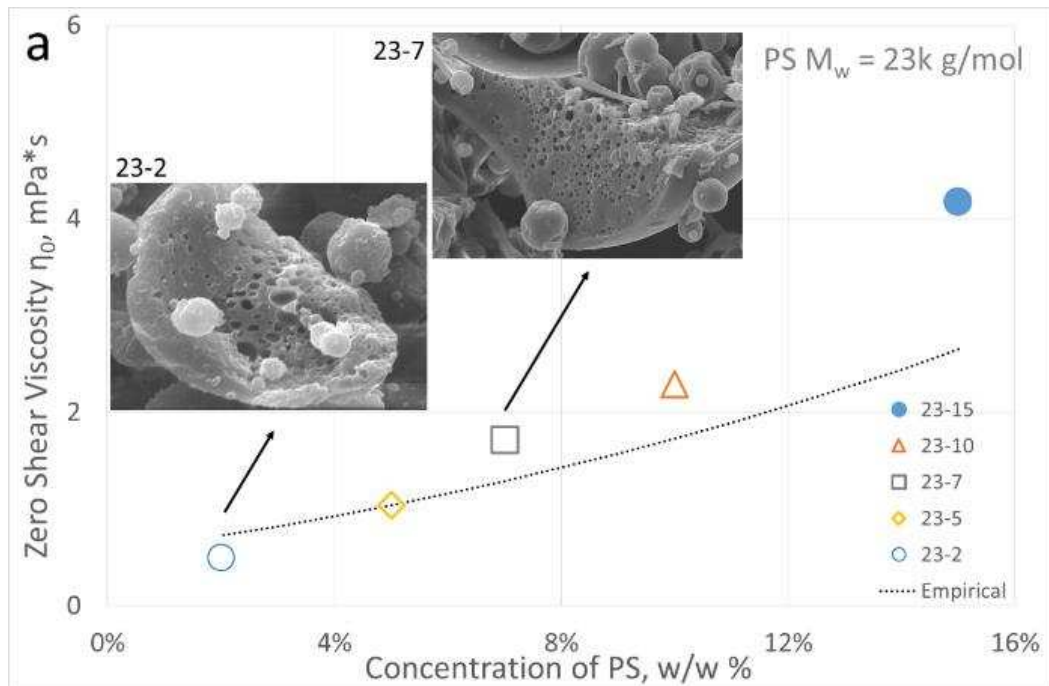
where l is the carbon-carbon bond length of the polystyrene skeleton (0.154 nm), θ is the tetrahedron angle (70.53°) and N is the number of repeat units in the polymer chain, calculated as molecular weight M_w of polystyrene divided by the molecular weight M_u of the monomer styrene unit (104.15 g mol⁻¹). Thus, R_g calculated from equation 5 was used for the C^* calculations (equation 4). The results show (Table 1 and Table 2) that both approaches predict a similar behaviour for the studied systems. There is a slight difference observed for the high molecular weight solutions (Table 2, compositions highlighted by patterned boxes). Results of the first approach (Table 1) based on literature values were used in the further analysis.

Table 2. C^* estimation using the values of R_g calculated from the Kuhn length and the contour length of polystyrene.[28] In the orange boxes the systems with concentrations above the critical chain overlap concentration, where the phase separation process is kinetically controlled. The composition demonstrating slight deviations of C^* from the previous method (Table 2) are highlighted by the patterned boxes. B = Below C^*, A = Above C^*.

PS Mw	R_g / nm	C^* / g cm³	2%	5%	7%	10%	15%
23k	3.93	0.150	B	B	B	B	A
bi-modal 53k and 107k	5.97 and 8.48	0.099 and 0.070	B	B	B	B/A	A
207k	11.79	0.050	B	B	A	A	A
317k	14.57	0.041	B	A	A	A	A

Viscosity of polystyrene-toluene-ethanol ternary systems:

Solutions of polystyrene in toluene at the initial concentrations of 2, 5, 7, 10 and 15% w/w were prepared for each of the polystyrene molecular weights. Zero shear viscosity η_o data was then obtained.
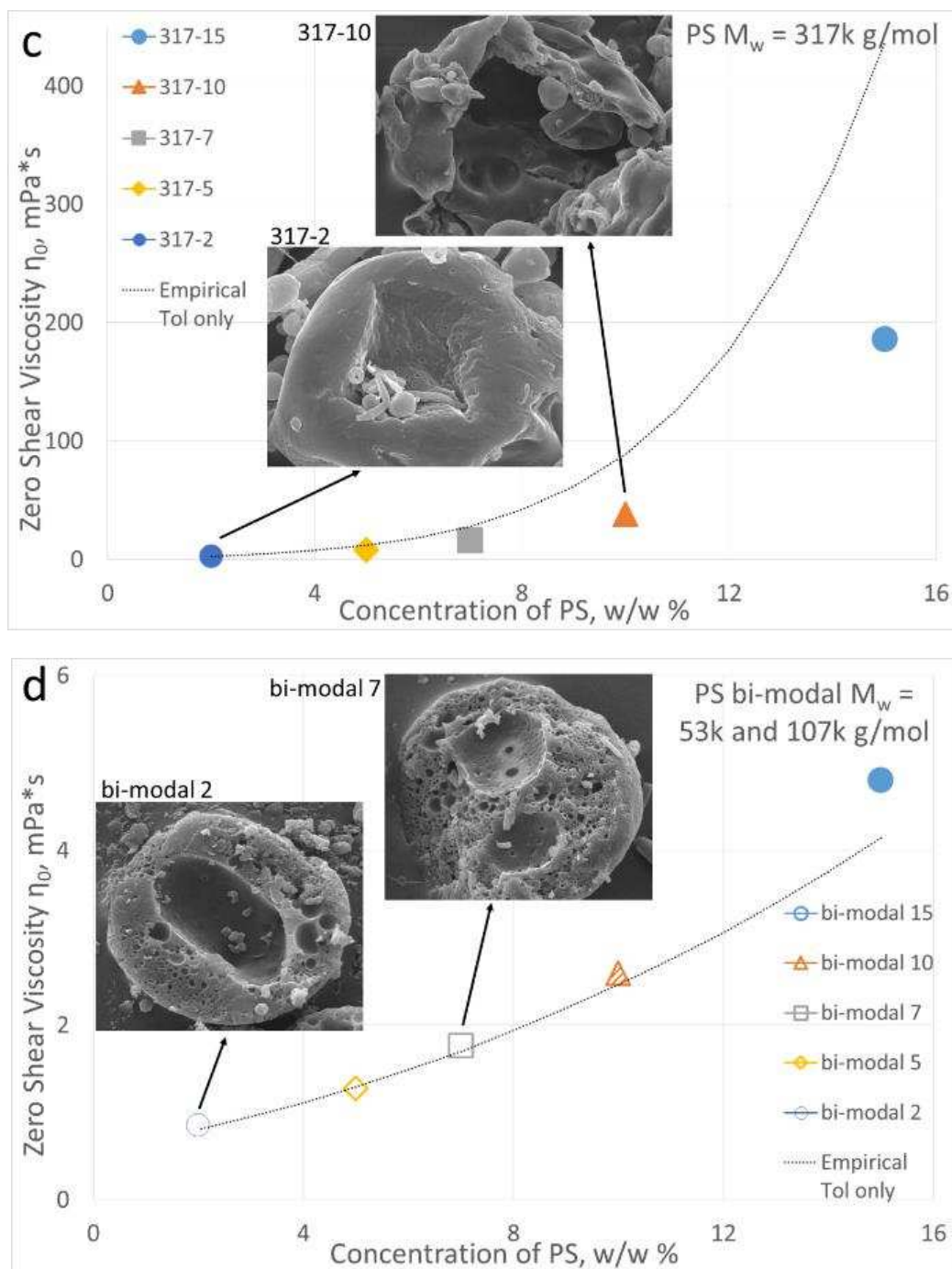
Figure 4. Zero shear viscosity η_o versus polystyrene concentration measured for polymer solutions with M_w = 23 kg mol^{-1} (a), 207 kg mol^{-1} (b), 317 kg mol^{-1} (c) and bi-modal 53 and 107 kg mol^{-1} (d). Filled symbols represent concentration above C^* where polymer chains entanglement occurs and the phase separation is kinetically controlled. Open symbols represent concentrations below C^*. The hatched symbol for "bi-modal 10" indicates that only the long chains of the bi-modal sample are above C^*. The dotted line was obtained using an empirical relationship between zero shear viscosity, polystyrene molecular weight and polystyrene concentration for

polystyrene-toluene systems from literature (equation 7)[29]. The relationship predicts the zero shear viscosity of polymer-solvent solutions. Inserts show representative SEM cross-section images of polystyrene particles obtained from these solutions.

A dotted-line overlapping the experimental data was generated by using an empirical equation from literature[29] that relates the zero shear viscosity η_o of polystyrene-toluene systems to polystyrene molecular weight M_w and polystyrene concentration C:

$$\eta_0 = 4.81 \times 10^{-3} \times C \times Mw^{0.736} + 1.658 \times 10^{-5} \times C^2 \times Mw^{1.472} + 5.579 \times 10^{-13} \times$$
$$C^{4.55} \times Mw^{3.35} + 0.558 \tag{7}$$

The predicted viscosity is in good agreement with the experimental data for the low molecular weight polymer and for the high molecular weight polymer at low concentrations. Deviations are observed for the high molecular weights at higher concentrations.

Structural characterisation of the polystyrene particles by SAXS.

The polystyrene multi-voided particles were characterized by small angle X-ray scattering (SAXS). This allowed us to determine the mean pore diameter for a large number of particles and pores and as such is complementary to SEM. Scattered intensity of nanoscale structural objects at large q should follow a power law dependence:[30]

$$I(q) \propto q^{-P} \tag{8}$$

where P is the power-law exponent. In the particular case, when $P = 4$, eq. 8 corresponds to Porod's law, describing scattering from a two-phase system with sharp interfaces. It is expected that the studied polystyrene multi-voided particles in air correspond to a typical two-phase polymer-air system having sharp distinct interfaces. Indeed it was found that SAXS patterns of these particles obey Porod's law at large q (Figure 5). A complete expression for Porod's law is:[30][31]

$$I_v(q) = \frac{I(q)}{V} \propto \frac{2\,\pi\,(\Delta SLD)^2\,S_v}{q^4} = \frac{B}{V}\,q^{-4} = B_v\,q^{-4} \qquad (9)$$

where I is the relative scattered intensity, I_v is the absolute scattered intensity, V is the sample volume irradiated by X-rays, ΔSLD is the contrast corresponding to a difference between scattering length densities of the two phases, S_v is the total surface area per unit volume and B_v is Porod's constant per unit volume of the material. Another parameter to be considered in SAXS analysis of the system is the invariant. When expressed on an absolute scale the invariant is defined as the total scattering power of the sample per unit volume, calculated by integrating the absolute scattered intensity over the entire reciprocal space:[30][31]

$$Q_v = \frac{Q}{V} = \int q^2\,I_v(q)\,dq = 2\,\pi^2\,(\Delta SLD)^2\,\varphi_P(1 - \varphi_P) \qquad (10)$$

with φ_P being the volume fraction occupied by the air.

A relative Porod's constant B (eq 9) and the relative invariant Q (eq 10) can be used to calculate S_v:[30][31]

$$S_v = \frac{\pi\,B\,\varphi_P\,(1 - \varphi_P)}{Q} \qquad (11)$$

It should be noted that absolute intensity calibration of scattering patterns is not required for this calculation as only the ratio B/Q, excluding irradiated sample volume, is used in eq 11.

The air volume fraction (dominated by the pore volume fraction of the voided polystyrene particles) can be estimated knowing the density of polystyrene ρ_s, the density of air ρ_p and the packing density of the particles in the sample volume ρ_{sam}, measured as mass of the sample divided by the volume occupied:[30]

$$\varphi_P = \frac{\rho_s - \rho_{sam}}{\rho_s - \rho_p} \qquad (12)$$

The volume fraction occupied by polystyrene is the remaining volume:[30]

$$\varphi_s = 1 - \varphi_P \qquad (13)$$

17

Using the values for the surface area S_v and the pore and structural volume fractions φ_P and φ_s of the samples, it is possible to determine the pore chord l_p defined as the average length of the void domains:[30]

$$l_p = \frac{4\,\varphi_p}{S_v}$$

(14)

The B/Q ratio required for S_v and chord length calculations were obtained from SAXS patterns (Figure 5) using a one-level model of the unified approach[24] implemented in Irena SAXS macros.[23]
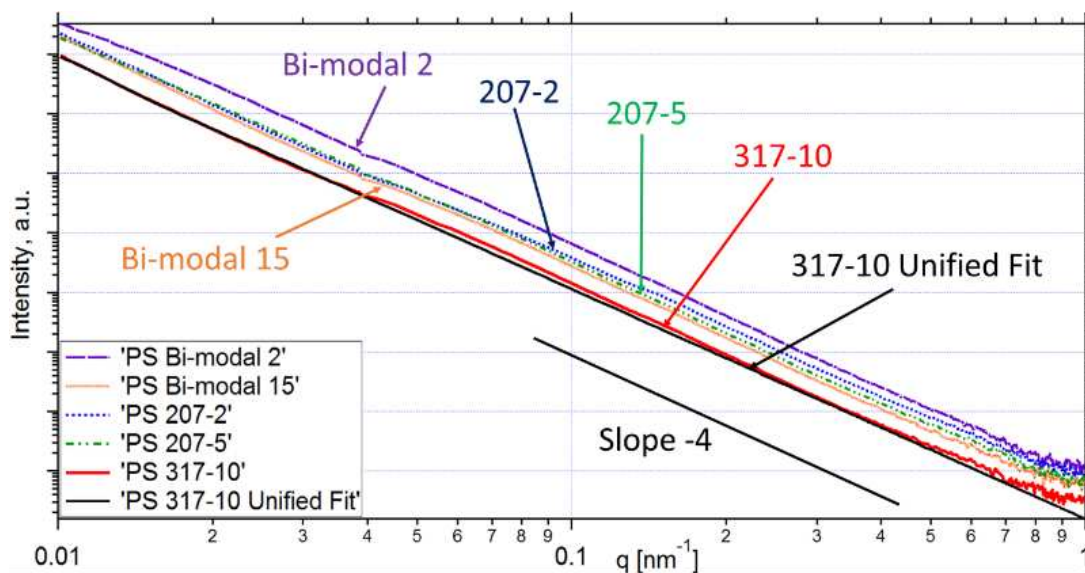

Figure 5. Representative SAXS patterns of polystyrene multi-voided particles, displayed in a double logarithmic format, acquired at the ID02 beamline. The patterns were fitted using a one-level model of the unified approach implemented in Irena SAXS macros for Igor Pro software. It was assumed for the model that at high q, $I(q) \propto q^{-4}$. The solid black line shows an ideal fit using the unified approach. The slope -4 line is given for guidance.

The results of SAXS analysis (Table 3) show that the surface area of the polystyrene particles ranges from 5.32 m²/cm³ for the sample "23-2" with lowest molecular weight (23 kg mol⁻¹) and lowest polystyrene concentration in toluene (2% w/w) to 0.97 m²/cm³ for the sample "317-10" with the highest molecular weight (317 kg mol⁻¹) and the highest polystyrene concentration in toluene (10% w/w). The results of SAXS analysis have shown that the pore size l_p ranges from 483 nm for "23-2" to 3452 nm for "317-10" and the voids volume fraction ranges from 55 to 84%.

Table 3. Results of the SAXS data analysis: sample packing density (ρ_{sam}), air volume faction (ϕ_p), interface surface area per unit volume (S_v) and pore chord length (l_p). The samples above C^* are indicated in bold.

Sample	Packing density ρ_{sam} (g x cm^{-3})	Air volume fraction φ_P / %	Surface area S_v (m^2 x cm^{-3})	Pore chord l_P (nm)
23-2	0.382	64	5.32	483
23-5	0.483	55	4.25	515
23-7	0.383	64	4.82	532
23-10	0.388	64	4.66	547
23-15	0.416	61	4.44	550
207-2	0.323	70	2.52	1109
207-5	0.205	81	2.07	1563
207-7	0.299	72	2.42	1191
207-10	0.373	65	3.00	869
207-15	0.384	64	2.38	1077
317-2	0.440	59	3.94	598
317-5	0.301	72	2.56	1121
317-7	0.334	69	2.42	1139
317-10	0.173	84	0.97	3452
bi-modal 2	0.278	74	4.35	680
bi-modal 5	0.263	75	3.92	769
bi-modal 7	0.384	64	2.74	935
bi-modal 10	0.367	66	2.07	1271
bi-modal 15	0.424	60	2.60	930

For low molecular weight systems (23 kg mol^{-1} and bi-modal 53, 107 kg mol^{-1}) below the chain overlap concentration C^*, a correlation between the polymer concentration in the solvent and pore chord can be identified: an increase in concentration corresponds to an increase in the average diameters of the void domains and a reduction in surface area.

In the systems with higher molecular weight (207 and 317 kg mol^{-1}) this trend is not observed, which is likely to the fact that the chain entanglement in these samples determines a kinetic dominance of the phase separation process.

Scanning Electron Microscopy of polystyrene particles.

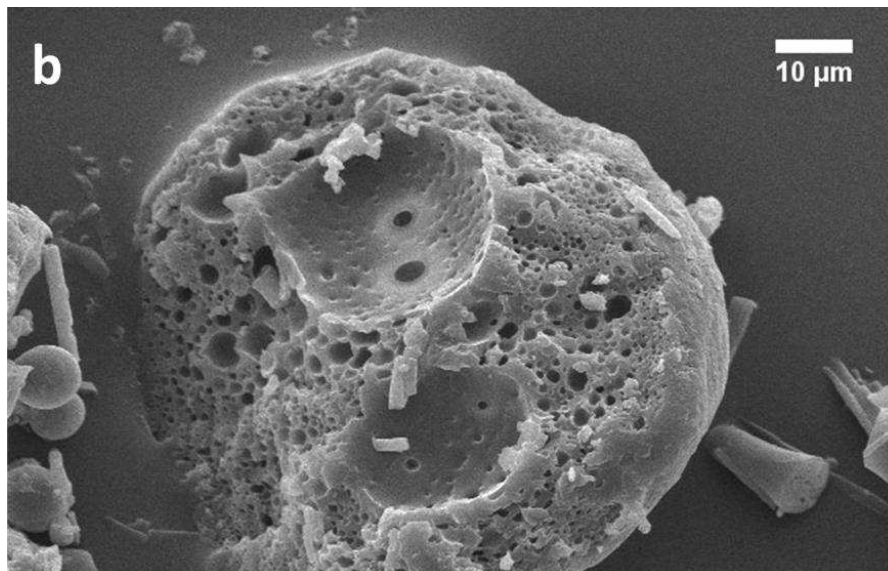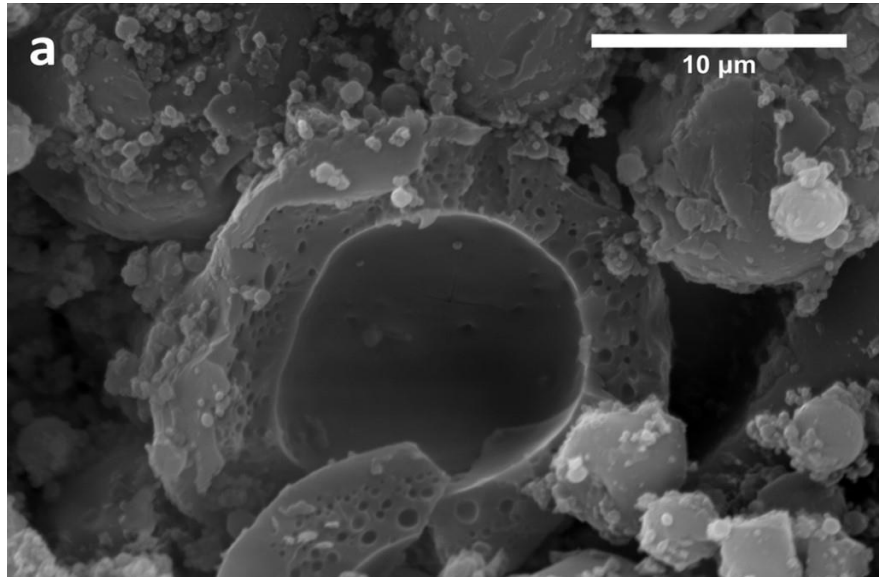Polystyrene particles were imaged using SEM and these are shown in Figures 6.

The particles display a spherical shape as they are formed from spherical droplets of polystyrene in toluene solutions dispersed as an oil-phase within the aqueous emulsions. Their size was comparable with the droplets size measured by DLS.

The particles presented a smooth external skin with closed internal pores, the result of nucleation and growth processes during the phase separation. A distribution of pore size within the particles was observed, with smaller pores located in proximity of the external regions and a large cavity towards the centre. This pore distribution is a consequence of the phase separation mechanism that starts from the external regions of the droplets forming the particles' smooth skin. Since the surface is quickly frozen by the loss of solvent and less mobile than the central region, during the solvent loss polystyrene will migrate from the centre to conserve density. This results in a large central cavity, as shown in the cross section of the sample "23-5" (Figure 6a).

A similar configuration is observed in the cross-section of the sample "bi-modal 7" (Figure 6b), with small pores near the outer surface and larger cavities towards the centre. It should be noted that the two populations of pores observed by SEM were not considered in the SAXS analysis. However, we expect the effect of these large cavities on the surface area derived from modelling the SAXS to be small. Assuming that the diameter of the cavities is about 20 times larger than the diameter of small pores (Figure 6a) and that the volume fraction of both the cavities and the small pores is equal, the cavities would contribute 5% of the total surface area corresponding to these two populations.

Particles produced by systems with significantly higher molecular weight (317 kg mol^{-1}) and concentration above *C**, exhibited a different morphology characterised by a considerably larger central cavity contained

within a relatively thin porous shell. This type of structure is clearly observable in the "317-10" sample in Figure 6c, where the cross section of the sphere reveals a large empty volume encompassed within a thin layer of polystyrene. The porosity observed within the thin shell of this particle, presenting a morphology that resembles an open porous network, is possibly produced by spinodal decomposition.
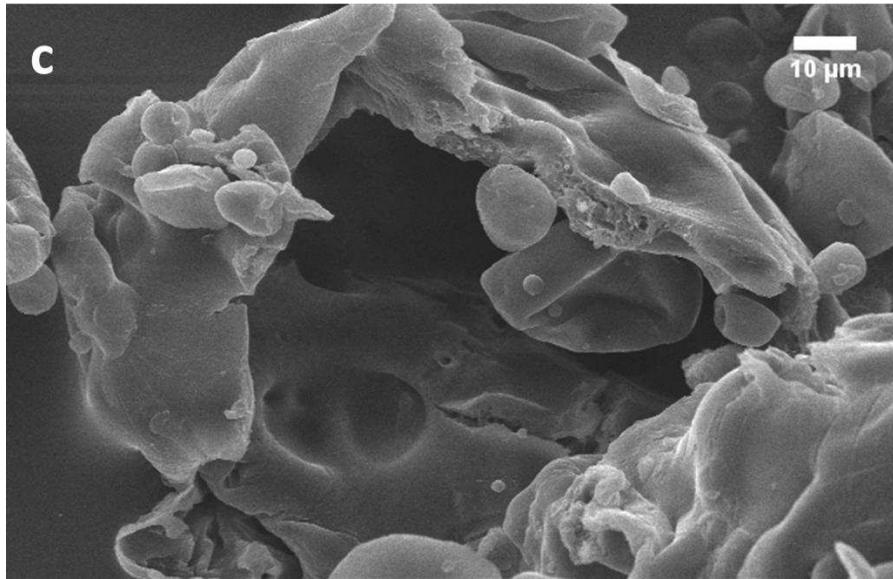
Figure 6 (a). A cross-section of a polystyrene micro-sphere produced by using PS M_w of 23 kg mol^{-1} and 5% w/w PS concentration (sample 23-5), below C^*. (b) bi-modal PS M_w of 53, 107 kg mol^{-1} and 7% w/w PS concentration (sample bi-modal 7), below C^*. (c) PS M_w of 317 kg mol^{-1} and 10% w/w PS concentration (sample 317-10), above C^*. Smaller pores are located in proximity of the external regions and a large cavity in the centre is present. The scale bars are shown on the images.

In order to estimate the pore size distribution within the samples and to compare the information obtained by SEM with the values for the average void size measured by SAXS (Table 3) the obtained images were processed using Image J[21] image analysis software.

The images selected were close-ups of the external regions of the particles, where most of the porosity was observed.
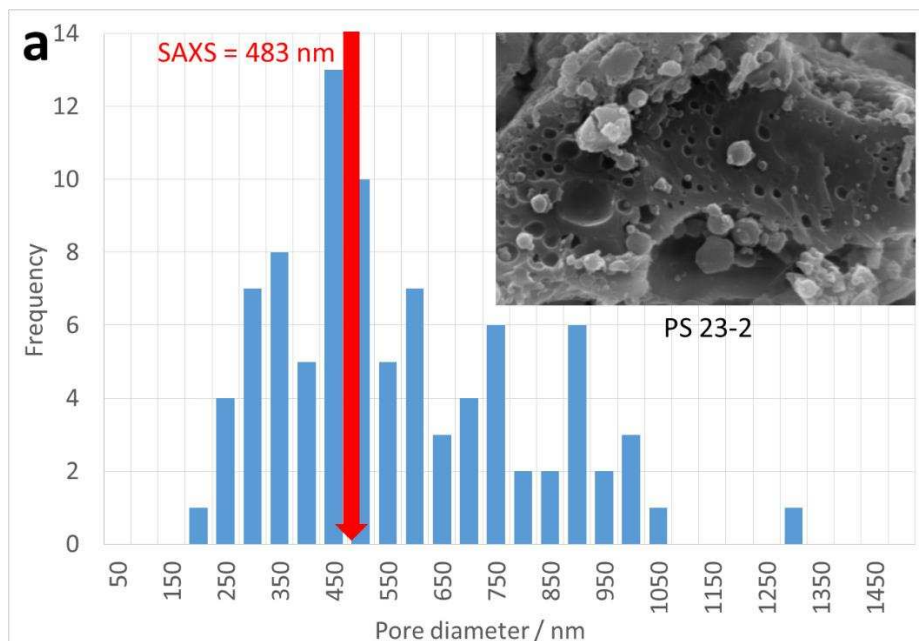
This analysis presented several limitations. Firstly, only small areas of the particles were considered. Therefore the images may not be representative of the entire sample. The image processing relied on the ability of the software to discriminate between pores (dark areas) and polymeric structure (light areas) by chromatic contrast. However, when this contrast was not particularly sharp, errors in determining pore size may be introduced. The assumption that pores were perfectly spherical was made and pore diameters were calculated from the area of the two-dimensional circular cross-sections. When a particle is fractured, spherical pores may be randomly cut at any section of the pore. Since the probability to be sliced in two perfect hemispheres is low, it is very likely that the almost entirety of the observed pores in the SEM images presented a diameter d smaller than the true diameter D of the void.

In order to account for this under-estimation of the pore diameters, a statistical correction was introduced. The equatorial diameter D of a spherical void is related to the diameter d measured from the SEM image by a parameter h, which represents the distance of d from the centre of the sphere.[32] The relationship between these parameters is given by the equation:[32]

$$h^2 = D^2 - d^2$$

(15)

Since the sectioning of a spherical pore can take place at any random distance h, the average probability value of h is equal to $D/2$. Solving equation 15 by replacing h with $D/2$ shows that the equatorial diameter D of a pore is given by $D = 2d / \left(3^{1/2}\right)$.[32] This correction was applied to convert all the measured diameters d into the equatorial diameters D.

Despite the number of assumptions made for SEM analysis, the pore size distributions of most of the samples estimated by this method was in a reasonably good agreement with the averaged void size obtained by SAXS analysis (Figure 7). The SAXS values fall within the pore-size distributions estimated by scanning electron microscopy, supporting the accuracy and complementary of the two different structural characterization techniques.
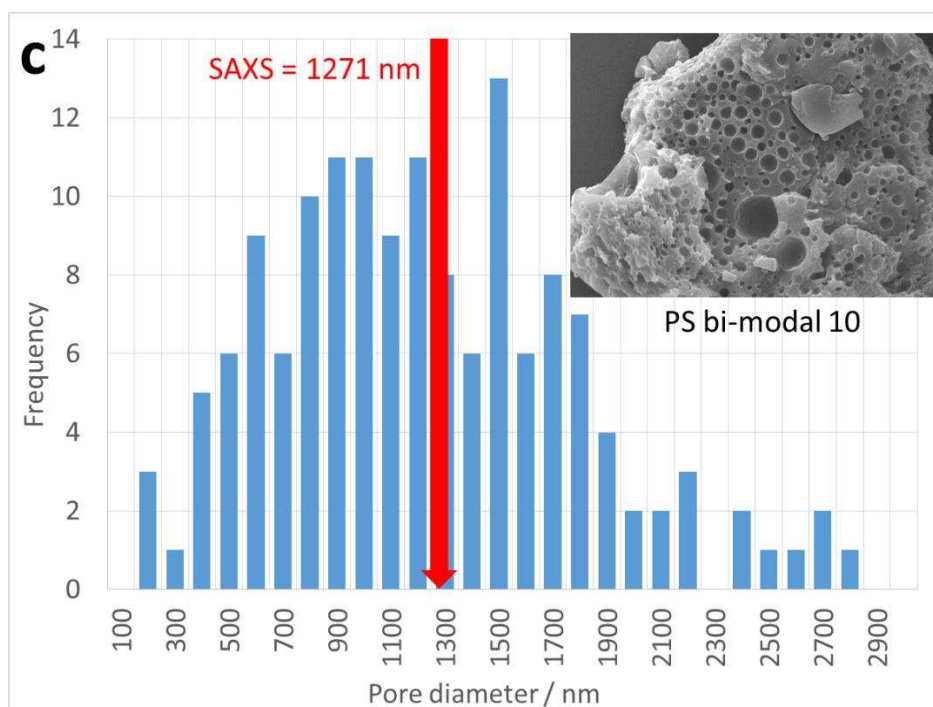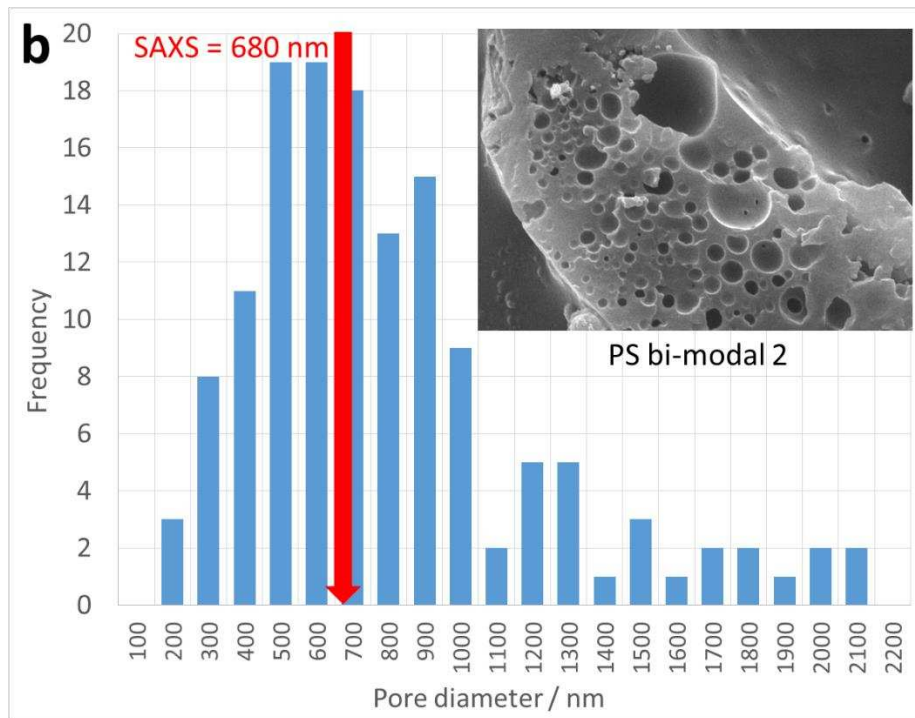
Figure 7. Histograms of the number of air voids (frequency) versus their diameter, showing pore size distributions obtained from 2D SEM images for cross section regions of the crushed samples "23-2" (a), "bi-modal 2" (b) and "bi-modal 10" (c). In the top corner of each diagram a representative SEM image that generated the distribution is shown. The vertical red arrows indicate the average size of the voids calculated by SAXS (Table 3).

Correlation between polymer concentration of polystyrene-toluene solutions and structural morphology of the particles.

Analysis of the structural information on particles' pore size obtained by SAXS measurements and supported by SEM imaging, together with the polymer concentration of the polystyrene-toluene solutions, has shown a strong correlation between these parameters (Figure 8). It was found that there is a linear dependence between 1/pore diameter and polystyrene concentration for the systems below C^*.

The linear trend is clearly observed for the 23 kg mol^{-1} and for the bi-modal polystyrene systems where most of the polymer solutions have concentrations below C^* (Table 1 and Table 2).

The samples that deviates from the linear trend are the samples prepared from 15% w/w polystyrene solutions. These are above C^*, where polymer chain entanglement takes place. For systems with concentrations above C^*, the proportionality relationship is no longer observed. The data points are scattered across the plot without an obvious trend.

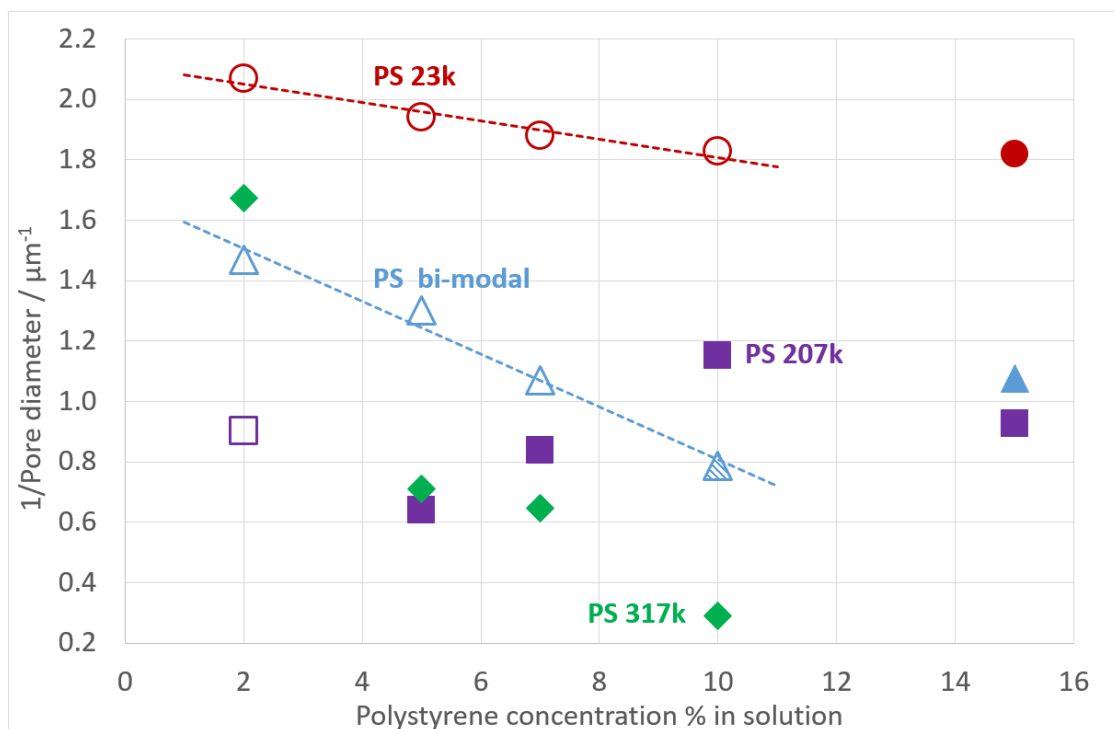Figure 8. 1/pore diameter vs polystyrene concentration in polymer solutions plot for the 23 kg mol^{-1} (circles), bi-modal 53, 107 kg mol^{-1} (triangles), 207 kg mol^{-1} (squares) and 317 kg mol^{-1} (diamonds) polystyrene systems. The open

symbols correspond to samples obtained from polystyrene-toluene solutions with polymer concentrations below C^* where the phase separation is thermodynamically controlled. Solid symbols represent polystyrene-toluene solutions with concentration above C^*, where the phase separation is kinetically controlled. The pattern-filled symbol for "bi-modal 10" shows that only the long chains of the bi-modal sample are above C^*. The diagram clearly highlights a linear correlation between 1/pore diameter and polystyrene concentration when $C < C^*$ in the 23 kg mol^{-1} and in the bi-modal systems. The correlation is no longer observable for 207 kg mol^{-1} and 317 kg mol^{-1} where $C > C^*$.

Since the viscosity of the polymer solutions used to fabricate the particles is proportional to the concentration of polystyrene in solution, an analogous linear trend is also observable between the zero-shear viscosity η_o of the polystyrene solutions and 1/pore diameter when $C < C^*$ (Figure 9).
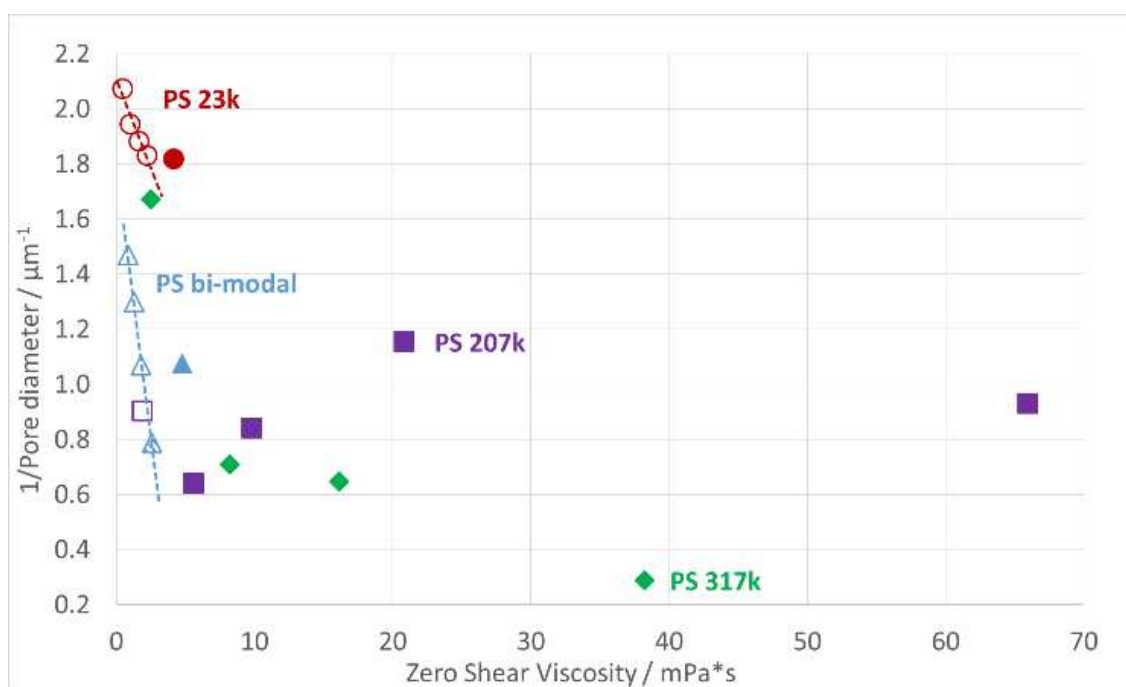

Figure 9. 1/pore diameter vs zero-shear viscosity η_o plot for the 23 kg mol^{-1} (circles), bi-modal 53, 107 kg mol^{-1} (triangles), 207 kg mol^{-1} (squares) and 317 kg mol^{-1} (diamonds) polystyrene systems. The open symbols correspond to samples obtained from polystyrene-toluene solutions with polymer concentrations below C^*, solid symbols represent polystyrene-toluene solutions with concentration above C^*, where the phase separation is kinetically controlled. The pattern-filled symbol for "bi-modal 10" shows that only the long chains of the bi-modal sample are above C^*. The diagram clearly highlights a linear correlation between 1/pore diameter and zero-shear viscosity η_o when $C < C^*$ in the 23 kg mol^{-1} and in the bi-modal systems. The correlation is no longer observable for 207 kg mol^{-1} and 317 kg mol^{-1} where $C > C^*$.

The observed reciprocal relationship between the polymer concentration and pore diameter, for polystyrene-toluene-ethanol systems when the concentration of the system is lower than the critical chain overlap concentration C^*, may have a practical application and could be used to produce porous polystyrene micro-spheres with "tunable" size voids.

Moreover, the correlation between pore diameter and zero shear viscosity demonstrated in this study could be used as a relatively simple tool to control the properties of the polystyrene-toluene-ethanol systems.

It could be predicted that when the glass transition temperature of the polymer intersects the temperature of the system upon the addition of the non-solvent, the phase separation arrests[19] and the morphology achieved at this stage is fixed. Since the glass transition temperature of a polymer in solution increases with increasing polymer concentration,[33] a polymer solution at high concentration of polystyrene is expected to intersect the temperature of the system in a shorter interval of time than a solution at low concentration of polystyrene. As a consequence, in a high concentration solution, phase separation would arrest earlier and produce pores of smaller size than in a low concentration solution. For systems with a fixed pore nucleation density, it would be expected to observe smaller pores (and consequently smaller surface area) in particles generated with high concentration solutions, and progressively larger pores (and larger surface area) in particles generated with low concentration solutions.

This trend of high concentration-small pores, is observed in polycarbonate in chloroform,[1] where increasing the polymer concentration produced monoliths with smaller pores.

However, the results obtained in the current study demonstrate the opposite trend, where polystyrene solutions with increasingly higher concentrations produced porous particles with increasingly larger pores (Figure 8). The glass transition behaviour alone is insufficient to justify the trend, but a deeper analysis of the phase diagram provides further insights about the processes taking place in these ternary systems, which could be helpful for the interpretation of the results.

A section of the ternary phase diagram (Figure 3) can be enlarged to highlight the region of interest (Figure 10). As a representative example the behaviour of only two polymer systems corresponding to M_w 23 kg mol⁻¹ and the bi-modal polystyrene at the initial concentrations of 2% and 7% w/w of polystyrene are considered. In this case, the starting conditions of the sample preparation (polystyrene in toluene solutions plotted on the polystyrene-toluene axis, represented as triangles), the final conditions reached upon ethanol addition

(squares) and the transition from the one-phase to the two-phase region (arrows) are clearly represented, along with the binodal boundaries.

The phase separation starts on crossing the binodal line: for the bi-modal systems this occurs in point A for the bi-modal-7 solution and in point C for the bi-modal-2 solution. Similarly it takes place in point B for the 23-7 solution and in point D for the 23-2 solution.
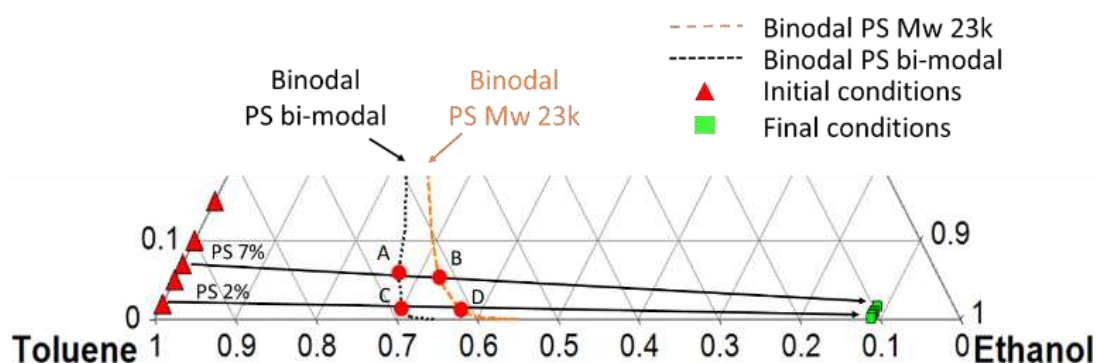

Figure 10. Section of the ternary phase diagram of Figure 3. The initial conditions are represented by the triangles on the toluene-polystyrene axis. The final conditions are represented by the squares. The binodal boundaries for the bi-modal and the 23 kg mol⁻¹ polystyrene are shown by dotted lines. The arrows represent the transition of the systems with initial polystyrene concentrations of 2% and 7% w/w from the one-phase to the two-phase region. The points A and C mark the starting points of phase separation of the bi-modal samples. The points B and D mark the starting points of phase separation for the 23 kg mol⁻¹ samples.

The compositions of the systems at these points are reported in Table 4 in the form of weight percentage of polystyrene, toluene and ethanol. The ratio of non-solvent to solvent (ethanol to toluene, ϕ_3/ϕ_1) is higher for low concentration polymer solutions [ϕ_3/ϕ_1 (C) > ϕ_3/ϕ_1 (A) and ϕ_3/ϕ_1 (D) > ϕ_3/ϕ_1 (B)]. At the same initial concentration, the solutions with lower molecular weight show a higher ethanol to toluene ratio [ϕ_3/ϕ_1 (B) > ϕ_3/ϕ_1 (A) and ϕ_3/ϕ_1 (D) > ϕ_3/ϕ_1 (C)].

Table 4. Composition of the systems at the points A, B, C and D (Figure 10) expressed in polystyrene, toluene and ethanol weight percentage. Ethanol to Toluene ratio (ϕ_3/ϕ_1), surface area of the particles generated by using these polymer solutions and the average pore diameters are also shown.

28

Sample	Point	PS wt%	Tol wt%	EtOH wt%	ϕ_3 / ϕ_1	Surface Area $(m^2 \times cm^{-3})$	Pore size (nm)
bi-modal 7	A	5.1	67.2	27.7	0.41	2.74	935
23-7	B	4.7	62.1	33.2	0.53	4.82	532
bi-modal 2	C	1.4	68.8	29.8	0.43	4.35	680
23-2	D	1.2	61.6	37.2	0.60	5.32	483

It could be concluded that a greater amount of non-solvent present in the system at the beginning of the phase separation process induces phase separation in a larger number of sites within the emulsion droplets: this results in a larger number of smaller pores in the particles generated by systems with higher ethanol to toluene ratio. This hypothesis is supported by SAXS results obtained for the particles surface area: larger ϕ_3/ϕ_1 corresponds to larger S_v, suggesting that a larger number of voids is present within these particles. As a result, the samples with larger surface area have voids with smaller average diameters. The ternary diagram (Figure 10) suggests that the relative concentration of non-solvent ethanol at the point of phase separation reduces either with the increase of polystyrene concentration or with the increase of polymer molecular weight. Thus, it should be expected that the pore surface area has to be reduced (and, consequently, the pore size has to be increased) either with an increase of molecular weight at a constant concentration of polymer (Table 4, compare samples bi-modal 2 and 23-2 or bi-modal 7 and 23-7) or with an increase of concentration for the same molecular weight (Table 4, compare samples 23-2 and 23-7 or bi-modal 2 and bi-modal 7). It should be noted that this conclusion is only valid for the porous particles obtained from solutions with polymer concentrations below C^*.

CONCLUSIONS.

This work explored the fabrication of porous polystyrene micro-spheres from ternary systems of polystyrene-toluene-ethanol by a process of non-solvent induced phase separation. A ternary phase diagram for the system was constructed and the boundaries between one-phase and two-phase regions were experimentally determined by turbidimetric titration for polystyrene within a wide range of molecular weights from 23 to 317 kg mol^{-1}.

Critical chain overlap concentrations C^* were estimated employing two different approaches, where the values for the radius of gyration of polystyrene were obtained from literature and also via the Kuhn length

and the contour length of a polystyrene chain in a theta solvent. These two approaches gave good agreement. The viscosities of polystyrene-toluene-ethanol mixtures were measured and the values of zero shear viscosity determined. The polystyrene micro-spheres were characterised by scanning electron microscopy and small angle X-ray scattering techniques, providing comparable information on the size of the internal voids.

It was found that the average size of the voids present in the porous structures is linked to the concentration of polymer in the polystyrene-toluene systems by a reciprocal correlation between pore diameter and polymer concentration. This reciprocal correlation is only valid for ternary systems with polymer concentrations below the critical chain overlap concentration C^*. Above C^* this relationship breaks down.

The reciprocal dependence between pore diameter and polymer concentration established for systems below C^* can be used to control void size during the production of porous polystyrene micro-spheres.

We also clarify that the observed relationship between 1/pore diameter and polymer concentration correlates well with the relative amount of non-solvent present in a system at the beginning of the phase separation process, as this induces more nucleation sites. The pore size can be reduced and, consequently, the pore surface area can be increased either by reducing polymer concentration in the initial solution or by decreasing polymer molecular weight in the sample composition.

ACKNOWLEDGMENTS:

CONFLICTS OF INTEREST:

We are not aware of any conflict of interest.

REFERENCES:

(1)   Xin, Y.; Fujimoto, T.; Uyama, H. Facile Fabrication of Polycarbonate Monolith by Non-Solvent Induced Phase Separation Method. *Polym. (United Kingdom)* **2012**, 53, 2847–2853.

(2)   Wang, D. M.; Lai, J. Y. Recent Advances in Preparation and Morphology Control of Polymeric Membranes Formed by Nonsolvent Induced Phase Separation. *Curr. Opin. Chem. Eng.* **2013**, 2, 229–237.

(3)   Kim, J.; Yaszemski, M. J.; Lu, L. Three-Dimensional Porous Biodegradable Polymeric Scaffolds Fabricated with Biodegradable Hydrogel Porogens. *Tissue Eng. Part C. Methods* **2009**, 15 (4), 583–594.

(4)   Rezabeigi, E.; Wood-Adams, P. M.; Drew, R. A. L. Production of Porous Polylactic Acid Monoliths via Nonsolvent Induced Phase Separation. *Polym. (United Kingdom)* **2014**, 55 (26), 6743–6753.

(5)   Johnson, D. W.; Langford, C. R.; Didsbury, M. P.; Lipp, B.; Przyborski, S. A.; Cameron, N. R. Fully Biodegradable and Biocompatible Emulsion Templated Polymer Scaffolds by Thiol-Acrylate Polymerization of Polycaprolactone Macromonomers. *Polym. Chem.* **2015**, 6 (41), 7256–7263.

(6)   Jinhua, L.; Dongliang, L.; Honghua, W.; Guangyuan, Z. Porous Polyethylene Spheres with Nanofiber Structure from Ziegler-Natta Catalyst Supported on Porous Polymer Particles. *Polymer (Guildf).* **2011**, 52 (3), 602–605.

(7)   Wang, Z.; Bai, R. Preparing Microgranules from Waste Polystyrene through a Novel Temperature- and Nonsolvent-Induced Phase Separation Method for Potential Adsorbent. *Ind. Eng. Chem. Res.* **2005**, 44 (4), 825–831.

(8)   Ahuja, G.; Pathak, K. Porous Carriers for Controlled/modulated Drug Delivery. *Indian J. Pharm. Sci.* **2009**, 71 (6), 599–607.

(9)   Chang, H. H.; Chen, S. C.; Lin, D. J.; Cheng, L. P. Preparation of Bi-Continuous Nylon-66 Porous Membranes by Coagulation of Incipient Dopes in Soft Non-Solvent Baths. *Desalination* **2013**, 313, 77–86.

(10)   Hong, Yi; Gao, Changyou; Shi, Yanchao; Shen, J. Preparation of Porous Polylactide Microspheres by Emulsion-Solvent Evaporation Based on Solution Induced Phase Separation. *Polym. Adv. Technol.* **2005**, No. 16, 622 – 627.

(11)   Guillen, G. R.; Pan, Y.; Li, M.; Hoek, E. M. V. Preparation and Characterization of Membranes Formed by

Nonsolvent Induced Phase Separation: A Review. *Ind. Eng. Chem. Res.* **2011**, *50*, 3798–3817.

(12)   Silverstein, M. S.; Cameron, N. R.; Hillmyer, M. *Porous Polymers*; 2011.

(13)   Ehsan Rezabeigi, Paula M. Wood-Adams, R. A. L. D. Isothermal Ternary Phase Diagram of the Polylactic Acid-Dichloromethane-Hexane System. *Polymer (Guildf).* **2014**, *55* (14), 3100–3106.

(14)   Yang, J.; Li, D. W.; Lin, Y. K.; Wang, X. L.; Tian, F.; Wang, Z. Formation of a Bicontinuous Structure Membrane of Polyvinylidene Fluoride in Diphenyl Ketone Diluent via Thermally Induced Phase Separation. *J. Appl. Polym. Sci.* **2008**, *110* (1), 341–347.

(15)   Karimi, Mohammad; Kish, M. H. Poly(methyl Methacrylate) Membrane: Dynamic Measurement of Concentrations During Water-Induced Phase Separation. *Macromol. Symp.* **2009**, *279*, 210–220.

(16)   Tanaka, H. Viscoelastic Phase Separation. *J. Phys. Condens. Matter* **2000**, *12* (15), R207–R264.

(17)   Altena, F. W.; Smolders, C. A. Calculation of Liquid-Liquid Phase Separation in a Ternary System of a Polymer in a Mixture of a Solvent and a Nonsolvent. *Macromolecules* **1982**, *15* (6), 1491–1497.

(18)   C. C. Hsul and J. M. Prausnitz. Thermodynamics of Polymer Compatibility in Ternary Systems. *Macromolecules* **1974**, 7 (3), 320–324.

(19)   Wang, Lawrence K.; Chen, Jiaping Paul; Hung, Yung-Tse; Shammas, N. K. *Membrane and Desalination Technologies*; Humana Press Inc.: Totowa, NJ, 2011.

(20)   Mark, J. E. *Physical Properties of Polymers Handbook*; 1997; Vol. 44.

(21)   Abràmoff, M. D.; Magalhães, P. J.; Ram, S. J. Image Processing with imageJ. *Biophotonics International*. 2004, pp 36–41.

(22)   Schneider, C. a; Rasband, W. S.; Eliceiri, K. W. NIH Image to ImageJ: 25 Years of Image Analysis. *Nat. Methods* **2012**, *9* (7), 671–675.

(23)   Ilavsky, J.; Jemian, P. R. Irena: Tool Suite for Modeling and Analysis of Small-Angle Scattering. *J. Appl. Crystallogr.* **2009**, *42* (2), 347–353.

(24)   Beaucage. Approximations Leading to a Unified Exponential/Power-Law Approach to Small-Angle Scattering. *J. Appl. Crystallogr.* **1995**, *28*, 717–728.

(25)   Ichiro Noda, Yuji Higo, Noboru Ueno, and T. F. Semidilute Region for Linear Polymers in Good Solvents.

Macromolecules **1984**, *17*, 1055–1059.

(26)   Fetters, L. J.; Hadjichristidis, N.; Lindner, J. S.; Mays, J. W. Molecular Weight Dependence of Hydrodynamic and Thermodynamic Properties for Well-Defined Linear Polymers in Solution. *J. Phys. Chem. Ref. Data* **1994**, *23* (4), 619–640.

(27)   Brandrup, J.; Immergut, E.; Grulke, E. A. Polymer Handbook. *John Wiley Sons, Inc* **1990**, *12* (3), 265.

(28)   Van Krevelen, D. W.; Te Nijenhuis, K. *Properties of Polymers*; 2009.

(29)   Kniewske, W. M. K. and R. The Shear Viscosity Dependence on Concentration, Molecular Weight, and Shear Rate of Polystyrene Solutions. *Rheol. Acta* **1984**, *23* (1), 75–83.

(30)   Hu, N.; Borkar, N.; Kohls, D.; Schaefer, D. W. Characterization of Porous Materials Using Combined Small-Angle X-Ray and Neutron Scattering Techniques. *J. Memb. Sci.* **2011**, *379*, 138–145.

(31)   Lindner, P.; Zemb, T. *Neutron, X-Rays and Light. Scattering Methods Applied to Soft Condensed Matter*; 2002; Vol. 5.

(32)   Barbetta, A.; Cameron, N. R. Morphology and Surface Area of Emulsion-Derived (PolyHIPE) Solid Foams Prepared with Oil-Phase Soluble Porogenic Solvents: Three-Component Surfactant System. *Macromolecules* **2004**, *37* (9), 3202–3213.

(33)   Burchard, W.; Ross-Murphy, S. B. *Physical Networks: Polymers and Gels*; Elsevier Science, 1990.